NEUTRON COMPUTED TOMOGRAPHY OF METEORITES: DETECTING HYDROGEN-BEARING MATERIALS. A. H. Treiman[1] , J. M. LaManna[2], L. M. Anovitz[3], D. S. Hussey[2] , and D. L. Jacobson.[2] [1]Lunar and Planetary Institute, 3600 Bay Area Blvd. Houston TX 77058 <treiman@lpi.usra.edu>, [2]National Institute of Standards and Technology, Gaithersburg MD. [3]Oak Ridge National Laboratory, Oak Ridge TN.

Introduction: Computed tomography (CT) from penetrating radiation allows one to reconstruct the interior structure of an object without physically dissecting it. Computed tomography using X-rays is becoming a standard technique in geological applications [1-5], and is being applied to planetary science to help target interesting materials [1,5]. Tomography using neutrons has, however, been used less in geological meteorite studies [6-8], and has the advantage for meteorites [2,9-12] of being sensitive to the presence and distribution of hydrogen, i.e., water or OH^-, with its implications for aqueous alteration processes in planetary bodies and potential habitability. Here, we present a preliminary evaluation of neutron computed tomography as a tool for detecting hydrogen-bearing materials in meteorites, and determining their spatial distributions.

Method and Samples: Neutron and X-ray computed tomographic (NCT, XCT) images were obtained at the National Institute of Standards and Technology (NIST) Center for Neutron Research (Gaithersburg MD), with their thermal Neutron Imaging Facility at BT2 using the NeXT system for simultaneous neutron and X-ray images [13]. The system uses thermal neutrons (i.e. < 25 meV) and X-rays of ~45 kV mean energy. Neutron flux is ~$5x10^6$ $cm^{-2}\cdot sec^{-1}$ for an L/d ratio of 600. The system produces 3D images of the distributions and intensities of neutron and X-ray attenuations (both scattering and absorption), with voxels of ~20 μm on a side. The NCT and XCT images are co-registered, and can be combined to a NXCT product.

Each NXCT tomograph requires approximately one day of irradiation, for a total neutron fluence of ~$5x10^{11}$ cm^{-2}. Samples are heated minimally (<1 $\mu Watt\cdot cm^{-2}$). Neutrons are scattered strongly by ^1H (scattering cross section, σ_s=83 barn); in geological samples, Fe is the next strongest bulk scatterer and absorber (σ_s=11 barn; absorption cross section, σ_a=2.6 barn) [14]; isotopes of some rare elements absorb neutrons very strongly (e.g., ^{157}Gd, σ_a=259000 barn; ^{149}Sm, σ_a=42080 barn), but are not expected to be apparent in our images.

As with neutron activation analysis, neutron capture during tomography will alter some isotope ratios. However, our NCT requires a neutron fluence many orders of magnitude smaller than that of typical neutron activation analyses, ~$5x10^{18}$ $n\cdot cm^{-2}$ (e.g., [15]). In the NCT here, neutron fluences affect the most sensitive isotope ratios (e.g., $^{158/157}Gd$, $^{150/149}Sm$) by less than a few parts in 10^7 [14].

GRA06100 is a CR2.8 chondrite, little weathered [16,17]. We were allocated fragment ‘,84’, 8.691 gm. It is mostly magnesian chondrules (Type 1) with abundant iron metal, ~12% phyllosilicate minerals [17], and a bulk H_2O content of 1.3%wt [18].

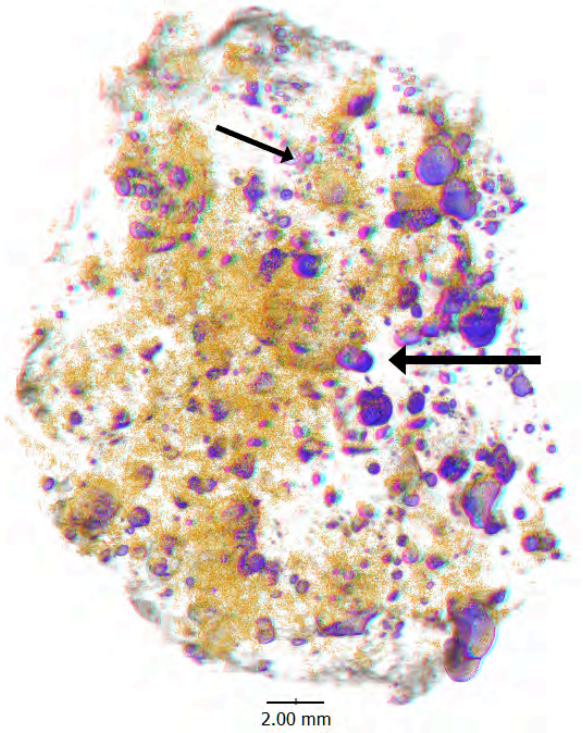

Figure 1. Red – cyan anaglyph from the NXCT images of GRA06100,84. Purple masses are Fe metal, from XCT, in and around chondrules. Thick arrow marks an Mg-rich (type 1) chondrule – a spherical ‘void’ space; thin arrow marks a possible Fe-rich (type 2) chondrule. Yellow shows neutron attenuation (from NCT), mostly from ^1H, representing patchy irregular distribution of H-bearing minerals (phyllosilicates, serpentines).

EET87503 is a howardite achondrite, little weathered [19,20]. We were allocated fragment ‘,73’, 11.098 gm. Like many howardites, it contains xenoliths of C-chondrite material [20-23], which contain ~1% H [18] in their serpentine and clay minerals (e.g., saponite).

Results: Our preliminary results show some of the possible uses of NXCT in analyzing meteorites.

GRA06100. NCT contrast for GRA06100 comes from both Fe and H (Figure 1). The abundant Fe-Ni metal is visible as chondrules (spheres) and chondrule components (rings and partial shells) in Fig. 2. Mg-rich, type 1, silicate chondrules appear as spherical

'voids' in NXCT, commonly marked by shells or exterior layers of Fe- and/or H- rich material (Figs. 1,2). Fe-rich, type 2, chondrules are distinguishable (Fig. 1). Contrast from H is irregularly dispersed [24], compare the NCT and XCT images of Fig. 3. ^{1}H is concentrated in diffuse bands or blotches, which may represent channels along which aqueous fluid flowed (Fig. 2).

EET87503. An NXCT anaglyph of EET87503 (Fig. 3) shows small grains of metal and discrete H-bearing regions, which are consistent with being C chondrite clasts [20-23]. Larger silicate clasts can be recognized, but without spatial details available from higher-voltage XCT systems [5]. Comparison of NCT and XCT images clearly distinguishes Fe-rich material from the hydrous C-chondrite clasts.

Conclusions: Neutron computed tomography can be an important tool for exploring the interiors of planetary materials, especially when accompanied by simultaneous X-ray tomography. NCT is most sensitive to

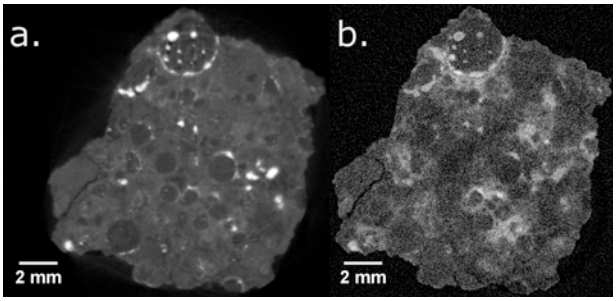

Figure 2. CT slices through GRA06100,84. (a.) X-ray CT; whitest spots are Fe metal. Round dark areas are Mg-rich (Type 1) chondrules, note their rims and inclusions of metal. (b.) Neutron CT; brightness reflects both Fe and H contents; compare with part a. Areas richer in H (which is concentrated in aqueous alteration minerals) are distributed patchily [24].

abundances of ^{1}H, i.e. substances containing H_2O or OH^-, but also detects Fe; simultaneous XCT will allows unambiguous discrimination of H-bearing regions. Thus NXCT can delineate distributions of volatiles in planetary materials, and allow them to be precisely targeted for detailed study.

Neutron tomography is minimally destructive of samples; it induces little heating, and (as done here) produces insignificant changes in isotope ratios and minimal residual radioactivity. As with any radiation method, neutron tomography will have some effects on target samples [25]; its effects must be evaluated in light of potential subsequent analyses. In any case, some aliquots of precious samples should be preserved unirradiated.

We are grateful to the Meteorite Working Group for approving our request for samples, and the Meteorite curatorial staff at ARES/JSC for rapid processing of the request.

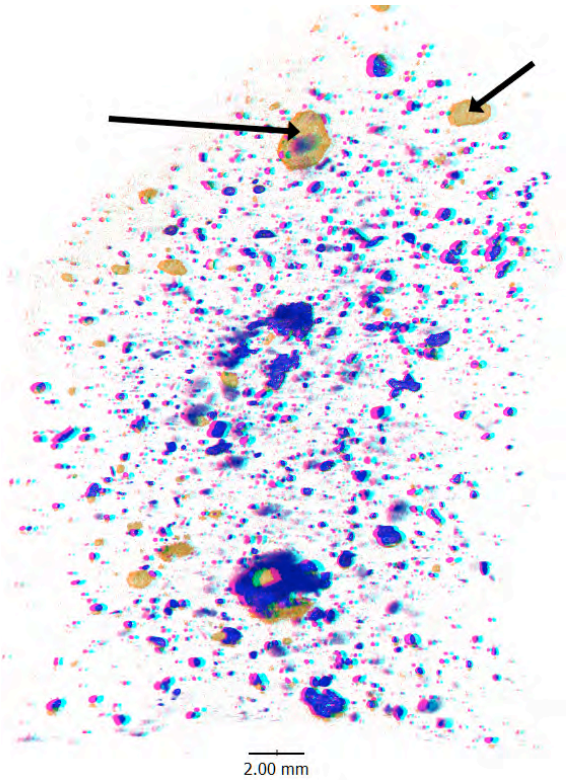

Figure 3. Red – cyan anaglyph from the NXCT images of EET87503,73. Purple masses are are Fe-rich metal and silicates, from XCT. Yellow masses (e.g., arrows) are H-rich, from NCT, and likely are fragments of C chondrites [20-23].

References: [1] Arnold J.R. et al. (1983) *Science 219*, 383-384. [2] Carlson W.D. (2006) *EPSL* 249, 133-147. [3] Mees F. et al. (2003) *Geol. Soc. London, Spec. Pub.* 215, 1-6. [4d Uesugi M., et al. (2010) *EPSL* 299, 359-367. [5] Zeigler R. et al. (2015) *6th NIPR Symp. Polar Science*, Mon. 15:15. [6] Winkler B. (2006) *Rev. Mineral. Geochem. 63*, 459-471. [7] Hess K.U. et al. (2011) *Geosphere* 7, 1294-1302. [8] Anovitz L.M. et al. (2016) *AGU Fall Mtg.* Abstr. H13F-1442. [9] Canella L. et al. (2009) *Appl. Radiation Isotopes 67*, 2070-2074. [10] Peetermans S. et al. (2013) *Analyst* 138, 5303–5308. [11] Caporali S. et al. (2016) *Minerals* 6, 14. [12] Pakhnevich A.V. (2016) *Brucker microCT users meeting Book 2016*, 219-228. [13] LaManna J.M. et al. (2017) *Rev. Sci. Instr. 88*(11), 113702. [15] Korotev R. et al. (2009) *MaPS* 44, 1287-1322. [14] Cross-sections from https://www.ncnr.nist.gov/resources/n-lengths/. [16] Righer K. et al. (2007) *Anarctic Meteorite Newsletter* 30,2. [17] Howard K.T. et al. (2015) *GCA* 149, 206-222. [18] Alexander C.M.O'D. et al. (2013) *GCA* 123, 244-260. [19] Righter K. & Garber J. (2011) *HED Compendium* https://curator.jsc.nasa.gov/antmet/hed/index.cfm [20] Buchanan P.C. & Mittlefehldt D.W. (2003) *Antarctic Meteorite Research* 16, 128-151. [21] Mittlefehldt D.W. et al. (2013) *MaPS* 48, 2105-2134. [22] Lorenz K.A. et al. (2007) *Petrology* 15, 109-123. [23] Zolensky M.E. et al. (1996) *MaPS* 31, 518-537. [24] Abreu N.M. & Stanek G.L. (2009) *LPSC* 40th, Abstr. #2393. [25] Sears D.W. et al. (2016) *MaPS* 51, 833-838.